Institutions of the Russian Academy of Sciences
Joint Institute for High Temperatures RAS
Institute of Problems of Chemical Physics RAS
Kabardino-Balkarian State University

Physics of Extreme States of Matter — 2011

Chernogolovka, 2011

Physics of Extreme States of Matter — 2011

Edited by academician Fortov V. E., Karamurzov B. S., Temrokov A. I., Efremov V. P., Khishchenko K. V., Sultanov V. G., Levashov P. R., Andreev N. E., Kanel G. I., Iosilevskiy I. L., Milyavskiy V. V., Mintsev V. B., Petrov O. F., Savintsev A. P., Shpatakovskaya G. V.

This compendium is devoted to investigations in the fields of physics of high energy densities and thermophysics of extreme states of matter. Interaction of intense laser, x-ray and microwave radiation, powerful particle beams with matter, techniques of intense energy fluxes generation, physics of shock and detonation waves, experimental methods of diagnostics of ultrafast processes, different models and results of theoretical calculations of equations of state of matter at high pressures and temperatures, low-temperature plasma physics, issues of physics and power engineering, as well as technology projects are considered. The majority of the works has been presented at the XXVI International Conference on Interaction of Intense Energy Fluxes with Matter (March 1–6, 2011, Elbrus, Kabardino-Balkaria, Russia). The edition is intended for specialists in physical and technical problems of power engineering.

The conference is sponsored by the Russian Academy of Sciences and the Russian Foundation for Basic Research (grant No. 11-02-06033).

ISBN 978-5-901675-96-0

Calculation results. We analyze the flat and droplet targets, homogeneous and nonhomogeneous in space, irradiated by CO_2 laser and Nd laser (1-, 2-, 3- harmonics) with different pulse duration and focal spot.

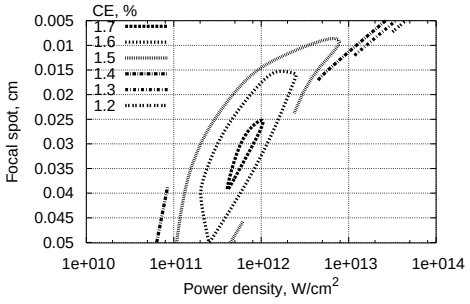

Figure 3. Conversion efficiency of gadolinium target (at 6.775 nm in 0.5% band) irradiated by Nd laser (first harmonic)

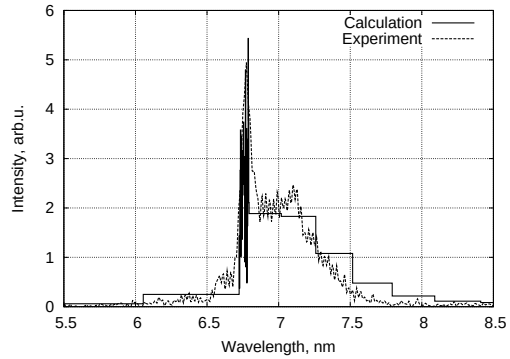

Figure 4. Calculated and experimental spectra for Gd plate irradiated by Nd laser (first harmonic) with energy 0.2 J, focal spot 200 mkm and Gaussian pulse with duration $\tau = 30$ ns

The results of detailed spectra calculations for homogeneous Gd droplet with radius $R = 100$ mkm are presented in Fig. 1. Figure shows, that with increasing the temperature the spectrum becomes more narrow and shifts to greater wavelengths.

In the Fig. 2 a comparison of Gd and Tb spectra for droplet with radius $R = 100$ mkm, electron density $N_e = 10^{20}$ g/cm^3 and temperature $T = 140$ eV are shown. One can see that Tb ($Z = 65$) spectrum is shifted in comparison to Gd ($Z = 64$) one approximately 0.2 nm to shorter wavelengths.

The conversion efficiency of Gd plate irradiated by Nd YAG laser (ie, yield of radiation in 0.5% band at $\lambda = 6.775$ nm divided by laser energy) in dependence over laser power density is shown in Fig. 3. As one can see from the picture, modelling by using the code RZLINE gives for solid flat Gd target CE $\sim 2\%$, which is in a good agreement with experiment.

Comparison of calculated and experimental spectra for the Gd plate irradiated by Nd laser (first harmonic) is given in Fig. 4.

It was Gaussian laser pulse with duration 30 ns, energy 0.2 J and focal spot 200 mkm. There were used only 100 spectral photon groups in radiation transport calculations, but it is sufficient to represent spectral data in narrow 0.5% band.

The work is supported by the Russian Foundation for Basic Research under Grant No. 09-01-00881.

1. EUV Sources for Lithography, Ed. V.Bakshi, SPIE, 1057p., 2006.
2. *Ivanov V.V., Novikov V.G., Solomyannaya A.D., Krivtsun V.M., Koshelev K.N.*, RZLINE MHD model of z-pinch discharge based EUV source, Proceedings of 2006 EUVL Symposium, Barcelona, Spain, October 16-18, 2006.
3. *Churilov S.S., Kildiyarova R.R., Ryabtsev A.N., and Sadovsky S.V.,* Phys. Scr. 80 (2009) 045303.
4. *Novikov V.G., Vorob'ev V.V., D'yachkov L.G., Nikiforov A.F.,* Influence of magnetic field on radiation of non-equilibrium plasmas of hydrogen and deuterium, JETP, 119(3), p.509-523, 2001.
5. *Nikiforov A.F., Novikov V.G., Uvarov V.B.*, Quantum-Statistical Models of Hot Dense Matter: Methods for Computation Opacity and Equation of State, Birkhauser, Basel, Switzerland, 428p., 2005.
6. *Novikov V.G., Koshelev K.N., Solomyannaya A.D.*, Radiative unresolved spectra atomic model, Physics of Extreme States of Matter, Chernogolovka, p.21-24, 2010.
7. *Novikov V.G., Solomyannaya A.D.*, Spectral properties of plasma consistent with radiation, High Temperature, 1998, v.36, N6, pp.858-864.

ELASTIC-PLASTIC PHENOMENA AND PROPAGATION OF STRONG SHOCK WAVES UNDER THE ACTION OF FEMTOSECOND LASER PULSES

***Inogamov N.A.*[1], *Khokhlov V.A.*[*1], *Zhakhovskii V.V.*[2]**

[1]*ITP RAS, Chernogolovka,* [2]*JIHT RAS, Moscow, Russia*

[*]*khokhlov@landau.ac.ru*

Investigation of the propagation of acoustic disturbances is of great theoretical and practical interest. The microinterferometry pump-probe laser pulse technique allowed to extend such studies to the scale $\sim 1 - 1000$nm and $\sim 0.1 - 100$ps. At the previous conference "Elbrus-2010" we have shown a good agreement of the experimental time profiles of displacement of rear surfaces of aluminum films in entering them disturbances, caused by influence of ultrashort laser pulses, with the theoretical calculations.[1, 2] However some dalay between experimental an calculated data was required to obtain this agreement. The further investigation has shown, that it is not connected with inaccuracy in determining the thickness of the film or fixing 0 time, and is a manifestation of a new effect of superelasticity.

Theoretical calculations were performed using a two-temperature hydrodynamic code (2T-hd) in which we used wide-range equation of state for aluminum by Khishchenko et al. [3, 4] Thus difference of crystals

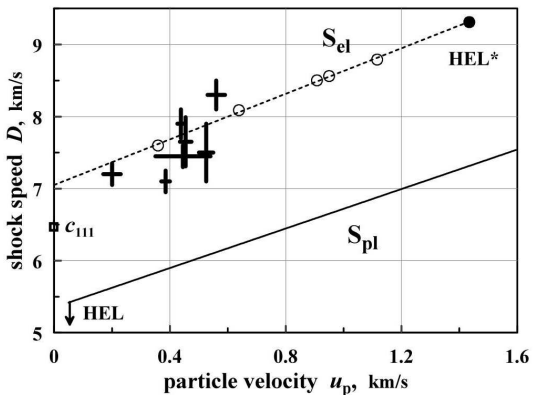

Figure 1. Comparison of elastic (S_{el}) and plastic (S_{pl}) Hugoniot with experiment[2, 5] (crosses).

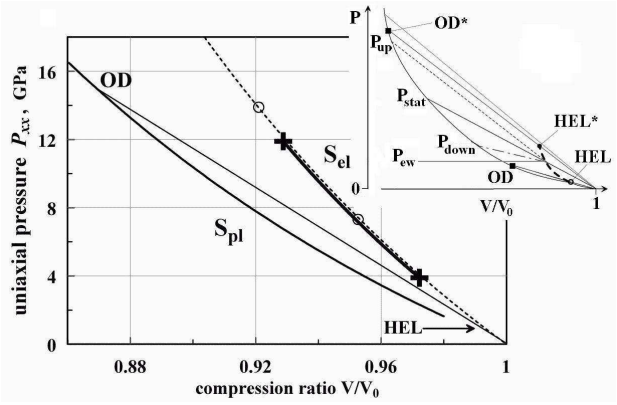

Figure 2. Elastic (S_{el}) and plastic (S_{pl}) shork adiabat curves. The corresponding to Fig. 1 segment of MD S_{el} covers the pressure range 7.4–33 GPa. Markers circles obtained by MD calculations. The lower circle with P = 7.4 GPa corresponds to the lower circle in Fig. 1

from liquids and plastic materials was not considered. In fact, the longitudinal sound speed in crystals $c_{el} = \sqrt{K + 4G/3)/\rho}$ is different for different crystallographic directions and exceeds the "plastic" sound speed $c_{pl} = \sqrt{K/\rho}$, where $K = -V\partial p/\partial V$ is the bulk modulus of elasticity, G is the shear modulus. The use of "plastic" equation of state did not raise the doubts since the characteristic values of the speed, deformation and pressure considerably exceeds the Hugoniot elastic limit (HEL), for Al p_{HEL} is less than ~ 1 GPa (see fig. 4 in [5]). However, the experimental values of the shock wave (SW) velocity were the relevant to the elastic sound speed.

In Fig. 1 by markers in the form of crosses are presented the data obtained in femtosecond laser experiments described in [2, 5] in comparison with the elastic (S_{el}) and plastic (S_{pl}) Hugoniot. Horizontal and vertical sizes of the crosses give the measurement error. For S_{pl} dependence $D_{pl} = c_{pl} + 1.37u_p$ (speed in km/s) approximates a large number of experimental data on aluminum [4], here u_p—the speed of particles of matter behind the shock front (piston speed), $c_{pl} =$ 5.35 km/s. All speeds are relative to a matter before the wave. The elastic adiabatic curve S_{el} shown on fig. 1 as straight line, passes through the circles, obtained by molecular dynamic (MD) simulations[6, 8] with the EAM (Embedded Atom Method) potential for aluminum, taken according to [7]. It is an elastic adiabatic curve of uniaxial shock compression on the direction 111. Its approximation looks like $D = c+ku_p$ with coefficients $c = 7.051$ km/s, $k = 1.581$.

On Fig. 2 adiabatic curves S_el and S_pl are shown on plane $P - V/V_0$. While plastic adiabat S_{pl} not limited to the high velocities and strains and goes into liquid adiabat at the intersection with the melting curve (the intersection is outside the frame of Fig. 1, 2), the elastic adiabat S_{el} passes over the marker HEL and is limited at the large amplitudes by the theoretical shear strength limit. This extension is allocated in Fig. 2 by bold strokes and ends with bounding marker as a solid circle HEL*. As shown in [8] for aluminum limit $p_{\mathrm{HEL}*} \approx 30$ GPa. In this sense, the ideal crystal behind the shock front, related to the segment of the elastic adiabat S_{el} between HEL and HEL*, is in a metastable elastically compressed state. Decay of the this state goes through formation, movement and multiplication of dislocations and, therefore, occurs at a time determined by the position in the interval between the HEL and HEL*. Thus there is a relaxation of the shear stress and the transition from elastic to plastic state. Typically his time is in the picosecond region. Close to HEL* uniaxial strain is so great that the crystal cell is destroyed in the shock front in a layer thickness of the order of several interatomic distances for the time the order of 0.1 ps. On the interval 0-HEL shock-compressed crystal is stable.

With the extension of the elastic adiabatic HEL for there is a possibility of a new regime of SW propagation: steady-state coexistence of the elastic and plastic waves. Stationary one-wave two-band configuration corresponds to the Rayleigh line, passing through three points (1,0), (v_{ew}, p_{ew}) and p_{stat} in Fig. 2 (ew-elastic wave). In this mode there are two zones—elastic and plastic. At constant pressure upon the piston p_{stat} ($p_{OD} < p_{stat} < p_{OD}*$) the distance d_{el} between elastic and plastic fronts does not change with time (stationary). The substance state in an elastic zone is presented by a point p_{ew} on Fig. 2. This state is on the continuation of an elastic shock adiabatic curve found in articles [6, 8] (fat strokes on Fig. 2). Elastic material is harder than plastically transformed material, respectively elastic adiabat is steeper than the plastic. Therefore, the straight line $(1, 0) - p_{ew} - p_{stat}$, first crosses the elastic shock adiabat. P_{stat} point belongs to the plastic shock adiabat. This point represents plastically transformed state behind front of a plastic wave.

Fig. 3 shows the velocity profiles of the substance of the MD (solid line) and 2T-hd (dashed line) calculations with conditions corresponding to the experiment [9]: aluminum foil, the absorbed energy $F_{abs} =$ 2.6 J/cm^2, the pulse duration $\tau_L = 0.12$ ps. Value $F_{abs} = 2.6$ J/cm^2 $= AF_{inc}$ corresponds to the intensity of the incident radiation $I_{inc} = 7.7 \cdot 10^{13}$W/cm^2. [9] In this MD calculation the crystal is oriented in the direction 110 relative to the axis of motion x. As the origin $x = 0$ the initial position the frontal boundary of

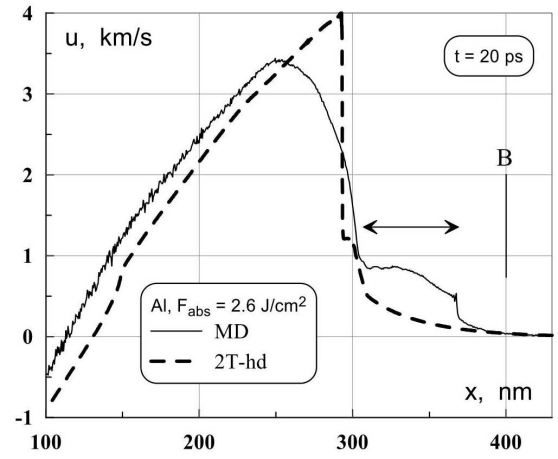

Figure 3. Joint distribution from left to right of an elastic precursor and plastic front at influence of an laser pulse with $I_{inc} = 7.7 \cdot 10^{13}\mathrm{W/cm^2}$ from work [9]. MD—a continuous curve, 2T-hd—a shaped curve. The elastic zone with the thickness $d_{el} = 70$ nm between an elastic shock wave (jump on the right) and plastic front (jump at the left) is noted by a bilateral horizontal arrow. The boundary between Al film $d_{film} = 400$ nm and glass is shown by vertical line B.

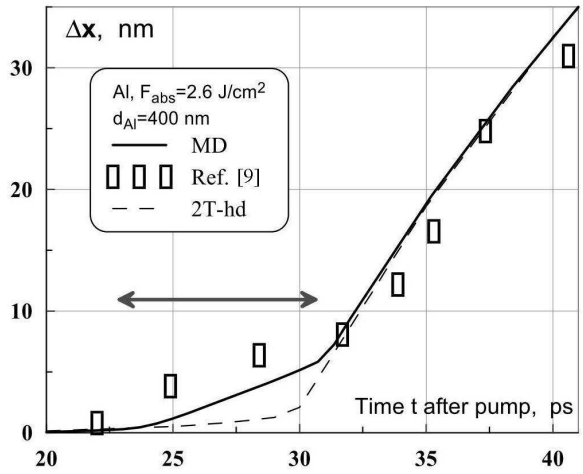

Figure 4. Displacement of the boundary with the glass Δx at passage of compression wave through the border. Horizontal arrow indicates elastic precursor.

the film is accepted. This boundary is exposed to the heating pulse. Concentration of randomly dispersed dot vacancies in the crystal before a wave is 10^{-3} per atom. Vacancies were introduced to assess the role of defects. In 2T-hd code the plastic equation of state [1–4] is used, therefore an elastic zone on the hydrodynamic profile is missing. MD simulation is agreed with the 2T-hd calculations on amplitude and width of the plastic compressed zone. Elastic p_{ew} and plastic p_{up} (see Fig. 2) pressures behind corresponding shock fronts at the moment shown in Fig. 3, are 20 and 93 GPa. This value p_{ew} about twice the value p_{ew}, reached in the experiments [2, 5].

As seen from Fig. 4 MD calculation (solid line) agrees well with the experimental data [9] (square markers). In 2T-hd calculation (dashed line) elastic precursor is absent. Note that in [9] the presence of the precursor was observed but its origin remains unexplained. Then it seemed an incredible idea of the existence of elastic effects in a large-amplitude waves. Calculated and experimental data agree by the time of exit of the precursor and the plastic wave on the film surface and the velocity of substance behind precursor and a plastic shock (0.7 km/s and 3–4 km/s, compare to the MD profile in Fig. 3). Thus experiment confirms the existence of the elastic precursor before the plastic jump with an amplitude of 1 Mbar.

Elasto-plastic configuration (solid curve in Fig. 3) is not steady. There are two sources of nonstationarity — it is, first, the attenuation of the shock wave as it propagates into the bulk of the target and, secondly, the interaction between elastic and plastic waves. Pressure $p_{up} = 93$ GPa behind plastic front in Fig. 3 above the stationary value $p_{stat} = 63$ GPa, which corresponds to the pressure $p_{ew} = 20$ GPa in a stationary configuration in Fig. 2. Thus the plastic Rayleigh line $p_{ew} \to p_{up}$ is steeper than the Rayleigh line $(1, 0) \to p_{ew}$ for an elastic jump (see Fig. 2). Therefore, the plastic front gradually approaches the elastic jump — the thickness d_{el} of elastic compressed zone is reduced. At times up to $t \sim 10$ ps, the distance d_{el} related to the width of the heated layer produced by the laser pulse at the two-temperature phase due to electronic heat conductivity. An elastic area is formed at the periphery of this layer. The minimum value of $d_{el} = 20$ nm is achieved at $t = 70$ ps, when the pressure p_{up} and p_{stat} compared. Thus elastic and plastic segments of the Rayleigh line forms a single straight line, see Fig. 2. Note that the minimum thickness $d_{el} = 20$ nm considerably exceeds the the lattice constant of 0.4 nm. At times $t > 70$ ps, the pressure behind the plastic shock is less than $p_{stat}(p_{ew} = 20\ \mathrm{GPa}) = 63$ GPa. Thus changes the sign of the angle between the segments of elastic and plastic Rayleigh lines. In Fig. 2, thare are line segments $(1, 0) \to p_{ew}$ and $p_{ew} \to p_{down}$. Now the elastic segment is steeper — the speed of elastic waves is higher: $p_{up} > p_{stat}$, $p_{down} < p_{stat}$, see Fig. 2. Hence, the plastic transformation front extends slowly than the elastic precursor. In this case, the thickness $d_{el}(t)$ of the elastic area starts to increase. For example, at $t = 200$ ps we have $d_{el} = 130$ nm. The corresponding plastic pressure $p_{down}(t = 200\ \mathrm{ps})$ is 30 GPa. It's interesting, that on the time interval up to $t = 200$ ps the pressure behind the plastic front decreases three times while the pressure behind the elastic jump and speed of this jump remain practically constant. They are $p_{ew} = 20$ GPa, and 8.6–8.8 km/s. In this the MD and 2T-hd simulations with high accuracy agree by an instant position of the plastic front and the pressure profile in the plastic zone. At a sufficient film thickness $\geq 3\mu$m pressure p_{down} gradually drops to p_{ew}. At this point the plastic wave stops. The thickness of the plastically transformed layer is determined by a point of stop. So, over time, dual-zone configuration of the elastic and plastic shock fronts degenerate into a powerful ($p_{ew} \gg p_{\mathrm{HEL}}$) purely elastic jump.

Submission of full plasticity of the shock wave has led to a misinterpretation of the interesting experi-

ments carried out in [10]. Experiments [10] carried out on aluminum at the same intensity of $7.7 \cdot 10^{13}$ W/cm^2, as in [9]. Above we have presented theoretical results related to the film thickness of 3–9 μm at this intensity. Calculations show that the interval 3–9 μm elastic jump passes at a speed of 8.7–8.3 km/sec. When the jump moves off to a distance $x = 9$ μm pressure behind the shock is 13 GPa. If, however, with with the authors of [10] assume that the jump is a plastic shock wave, then we come to a much greater pressure. This will need to obtain the observed in experiments [10] high average wave speed of about 9 km/s. According to the plastic shock adiabat it requires pressure behind the plastic shock of 70 GPa, even when the jump moves off to a distance of 9 μm.

This work was supported by the Russian Foundation for Basic Research, project no. 09-08-00969-a and Presidium of RAS program "Thermophysics and mechanics of extreme energy effects and physics of highly compressed matter"

1. Khokhlov V. A., Inogamov N. I., Anisimov S. I., Zhakhovsky V. V., Shepelev V. V., Ashitkov S. I., Komarov P. S., Agranat M. B., Fortov V. E. Investigation of two-temperature relaxation in thin foil on a glass substrate initiated by the action of ultrashort laser pulse // Physics of Extreme States of Matter—2010 / Eds. Fortov V. E., et al. Chernogolovka: IPCP RAS, 2010. P. 127–129.
2. Agranat M. B., Anisimov S. I., Ashitkov S. I., Zhakhovskii V. V., Inogamov N. I., Komarov P. S., Ovchinnikov A. V., Fortov V. E., Khokhlov V. A., Shepelev V. V. Strength properties of an aluminum melt at extremely high tension rates under the action of femtosecond laser pulses // JETP Lett. 2010. V. 91. P. 471. [Pis'ma ZhETF. 2010. V. 91. P. 517.]
3. Khishchenko K. V., Fortov V. E. // Physics of Extreme States of Matter—2002 / Eds. Fortov V. E., et al. Chernogolovka: IPCP RAS, 2002. P. 68–70; Levashov P. R., Khishchenko K. V. // AIP Conf. Proc. 2007. V. 955. P. 59–62.
4. http://teos.ficp.ac.ru/rusbank/
5. Ashitkov S. I., Agranat M. B., Kanel' G. I., Komarov P. S., Fortov V. E. Behavior of aluminum near an ultimate theoretical strength in experiments with femtosecond laser pulses // JETP Lett. 2010. V. 92. P. 516. [Pis'ma ZhETF. V. 92. P. 568.]
6. Zhakovskii V. V., Inogamov N. A. Elastic-plastic phenomena in ultrashort shock waves // JETP Lett. 2010. V. 92. P. 521. [Pis'ma ZhETF. 2010. V. 92. P. 574.]
7. Zhakhovskii V. V., Inogamov N., Petrov Y., Ashitkov S., Nishihara K. Molecular dynamics simulation of femtosecond ablation and spallation with different interatomic potentials // Appl. Surf. Sci. 2009. V. 255. P. 9592.
8. Zhakhovsky V. V., Budzevich M. M., Inogamov N. A., et al. // Science. (in preparation)
9. Evans R., Badger A. D., Fallies F., Mahdieh M., Hall T. A. Time- and space-resolved optical probing of femtosecond-laser-driven shock waves in aluminum // Phys. Rev. Lett. 1996. V. 77. P. 3359.
10. Huang L., Yang Y., Wang Y., Zheng Z., Su W. Measurement of transit time for femtosecond-laser-driven shock wave through aluminium films by ultrafast microscopy // J. Phys. D: Appl. Phys. 2009. V. 42. P. 045502.

NON-LINEAR EFFECTS IN THE FIELD OF INTENSE LASERS AND RADIATION OF RELATIVISTIC ELECTRONS

Khokonov M.Kh., Bekulova I.Z.***

KBSU, Nalchik, Russia

**khokon6@mail.ru*

Introduction Non-linear effects in interaction of ultra relativistic electrons with intense terawatt laser beam has first been studied experimentally in 1996, when first four harmonics were observed in electron radiation spectra [1]. Rapid progress in the creation of high-power lasers permits one to achieve at present time petawatt (10^{15} W) laser beams in the focus [2]. Such fields provide numerous drastic physical effects. Thus, high intensity colliding laser pulses can create abundant electron-positron pair plasma [3].

It was pointed out in [4] that quantum multi-photon radiation can be observable while few GeV electron collides head-on with a petawatt laser plane wave. Moreover such effect can take place within one laser wave period. In what follows we analyze such situations. It will be shown that an ordinary classical radiation theory approach permits one to describe the main futures of the basic electromagnetic processes like photon emission. The approach can naturally be generalized in order to take into account the quantum effects in photon emission like a radiation recoil as well as the influence of electron spin on radiation.

Theoretically high harmonic generation due to the interaction of intense laser waves with relativistic electrons based on classical electrodynamics was investigated recently in Ref.[5], where analytical formulas for the case of circularly polarized laser field have been obtained. We present here some more general approach which does not assume the laser beam to be a perfect plane wave, although numerical results are performed for liner polarized intense laser waves.

Classical radiation theory In order to gain physical insight without technical complications we start from relatively simple classical formulas. The spectral and angular distribution of energy radiated by a charged particle moving along a trajectory $\mathbf{r}(t)$ with velocity $\boldsymbol{\beta}(t) = \mathbf{v}(t)/c$ has the form [6]

$$\frac{d^2I}{d\omega d\Omega} = \frac{e^2\omega^2}{4\pi^2 c} \mid \mathbf{n} \times [\mathbf{n} \times \mathbf{j}_\omega] \mid^2, \qquad (1)$$

$$\mathbf{j}_\omega = \int_{-\infty}^{+\infty} \boldsymbol{\beta}(t) \exp(i\omega t - i\mathbf{rk}) dt, \qquad (2)$$

where ω and $\mathbf{k} = \omega\mathbf{n}/c$ are the frequency and wave vector of the radiation, and $d\Omega$ is the differential of the solid angle, c is the velocity of light.